A New Linear Ultrasonic Motor Using Hybrid Longitudinal Vibration Mode

XIANGYU ZHOU AND YI ZHANG
School of Advanced Manufacturing Engineering, Chongqing University of Posts and Telecommunications, Chongqing 400065, China

Corresponding author: X. Zhou (zhouxy@cqupt.edu.cn)

ABSTRACT This paper proposes a new linear ultrasonic motor using hybrid mode of the first symmetric and anti-symmetric longitudinal modes. The stator is constructed by two Langevin transducers in combination with two isosceles triangular beams. The triangular beams can transform the displacement in axial direction into the displacement in perpendicular direction and generate the oval trajectory of the driving foot, which is the merit of the simple structure. For better mode degeneration result, the influence of the triangular beam dimensions on the vibration frequency difference of the stator was analyzed by Finite Element Method (FEM) analysis. The overall dimensions of the prototype stator are 70 mm (length) × 15 mm (width) × 10 mm (thickness). Driven by ac signals with the driving frequency of 55 kHz and voltage 400 V_{p-p}, the motor can provide the no-load speed 63.87 mm/s and maximum thrust force 3.14 N, respectively. The frequency matching process of ultrasonic motor is simplified by adjusting the structure dimensions of the triangular beams.

INDEX TERMS Ultrasonic motor, piezoelectric transducer, hybrid mode.

I. INTRODUCTION

Ultrasonic motors (USMs) exhibit merits of small size, large torque in the low speed range, high positional accuracy, fast dynamic response and self-locking without electric power input [1]–[4], which are the weakness of electromagnetic motors. The working principle of piezoelectric USMs is to convert the electrical energy into mechanical oscillations of the stator based on the converse piezoelectric effect of piezoelectric ceramics, and to drive a moveable body by the friction force between the stator and the moveable body. During the past decades, USMs have been utilized in many fields, such as optical system, space explorations, ultra-precision measuring equipment, medical robot, etc. [5]–[7].

The bonded type [8], [9] and sandwich type (bolt-clamped type, the vast majority of sandwich type) [3], [10] are two typical structures of USM, which utilize the d_{31} and d_{33} working mode of PZT respectively. The transfer efficiency of the d_{33} mode of PZT is higher than that of d_{31} mode, theoretically [11]. Therefore, to acquire higher thrust force, output power and efficiency, the bolt-clamped type structure is a better choice for USM than the bonded type. And to improve the thrust force, some USMs [3], [4], [12] utilize two or more transducers to construct the stators. By comparison, the bonded type structure is suitable for miniaturization of USM without the limitation of bolt connection, but the output power and force are inevitably lower.

For most USMs, at least two modes are needed to be degenerated to excite the oval trajectory of the stator surface. And the eigenfrequencies of the two modes should be matched to be close in order to improve the output performance. Because that the tiny dimension deviation of the stator may cause an obvious eigenfrequency change of all modes and reduce the output performance, the frequency matching process of different modes is necessary and complicated in USM design process, especially for the complicated structure of stator constructed by multi transducers. Furthermore, affected by many other factors, such as PZT element, processing quality, it is hard to guarantee the consistency of matching results between the simulation model and the prototype [13].

Therefore, effective methods to simplify or avoid the frequency matching process and provide excellent frequency matching result are studied. The basic method is to change the frequencies of two necessary modes and minimize the frequency difference by adjusting the dimensions of the stator. For the USMs using hybrid vibration mode, such as longitudinal-bending mode [14]–[16], longitudinal-tortional mode [17], [18] and hybrid bending mode [19] and so on, the frequency matching process mainly covers the repeated adjustment of structure and dimensions of the stator.
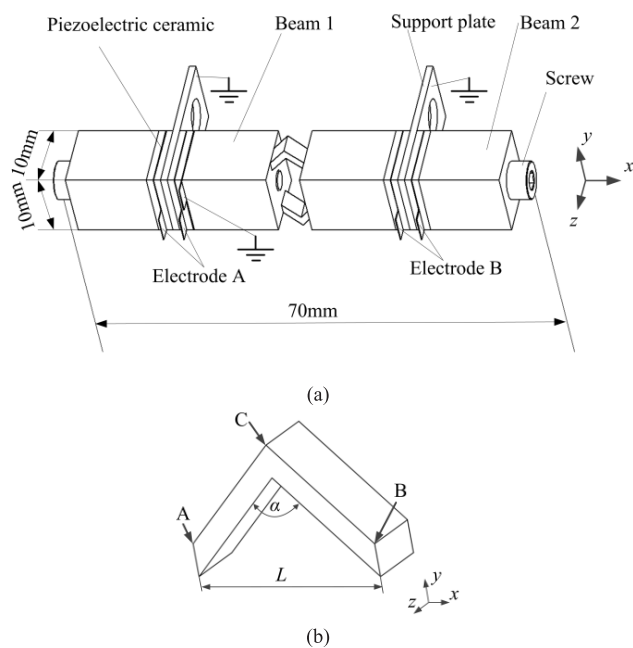
FIGURE 1. Structure of the stator: (a) Configuration; (b) Angle of the triangular beam.
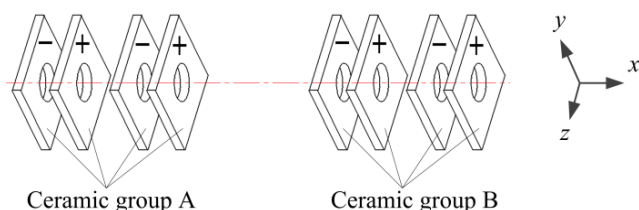

FIGURE 2. Arrangement of the polarized ceramics in axial direction.

However, the matching process can be simplified for some special structures with typical design methods.

One typical design method is to utilize the favorable vibration characteristics of structure symmetry. The symmetric structure can be classified into rotational symmetric structure and mirror symmetric structure. Many ultrasonic motors utilize the characteristic of rotational symmetric structure, which is the existence of the pair of orthogonal bending modes with same eigenfrequency, and generate travelling wave of ring-shape stator or superpose the two modes as the wobble operation mode of bar-shape stator to avoid the frequency matching process. The well-known SHINSEI USR series is a typical example motor with rotational symmetric structure [20]. A pair of orthogonal out-of-plane bending modes of the disk stator with close resonance frequencies can be excited to generate a travelling wave on the disk. In order to provide great torque with similar ring type structure of stator, Peng et al. [21] utilized the d_{33} working mode of PZT and provided an USM with sandwich type structure. The PZT components are welded on double sides along the ring stator. And two B-03 modes with similar frequency are excited to generate the travelling wave. The bar-shape wobble USM [22], [23] is another typical example with rotationally symmetric structure. Dong et al. [24] proposed a bar-shape USM for precision positioning, which can be excited into the rotating third-bending mode of the stator. In order to improve the thrust force, Shi et al. [25] utilized the d_{33} working mode of PZT and developed a linear ultrasonic motor with wheel-shaped bolt-clamped type stator, which excites a pair of orthogonal fourth-bending modes to generate the elliptical motion of two wheels.

Another typical design method is to connect multi transducers with low stiffness structure and construct symmetric stator. When two or more transducers are used to construct a stator, the vibration interference of them may generate complicated vibration modes, and the matching process is affected by more factors. Then, the mirror symmetric structure can be utilized to simplify the frequency matching process because of the possible existence of a pair of symmetric and anti-symmetric vibration modes with close eigenfrequency, which can be combined as a hybrid working mode. A typical example is the V-shape USM. Asumi et al. [12] proposed a V-shape USM, which is composed of two transducers. The longitudinal vibrations of two transducers interfere with each other and derive the symmetric and anti-symmetric vibration modes. To match the resonance frequencies of the two modes, the effects of three major dimensions were analyzed by FEM method, and the effect of friction material weight on frequency was also tested. Shi et al. [3] proposed a stator, which is constructed by two Langevin transducers connecting by a low stiffness beam, and provided an optimal design method based on Ansys parametric design language. To weaken the interference of transducers and expand the function of USM, a low stiffness triangular beam was used in the USM design by Zhou et al. [26]. Although the maximum thrust force is only 1.4N, the maximum frequency difference of two pairs of modes of the differential USM is only 0.15 kHz, which tested the effectiveness of low stiffness beam in frequency matching. In addition, some rotational symmetric structure USMs using longitudinal vibration mode of transducers have been reported for the reliable operation principle. Vasiljev et al. [27] connected four transducers by low stiffness beams as the stator of USM, and excited the longitudinal vibrations of them to achieve body's movement in the plane. Zhou et al. [28] excited the longitudinal vibrations of four transducers of the stator to acquire a pair of longitudinal vibration mode and realized the rotary driving function.

In this paper, a new bolt-clamped type USM is presented. To acquire enough thrust force and minimize the structure dimension of the USM, two bolt-clamped transducers with dimensions of 10 mm × 10 mm in cross section are used. And to reduce the vibration interference of the transducers, the low stiffness isosceles triangular beams are used to connect them, which also can transform the displacements of transducers in axial direction into the displacement of driving foot in perpendicular direction and generate the necessary oval trajectory of the foot for driving. The operation principle of the USM
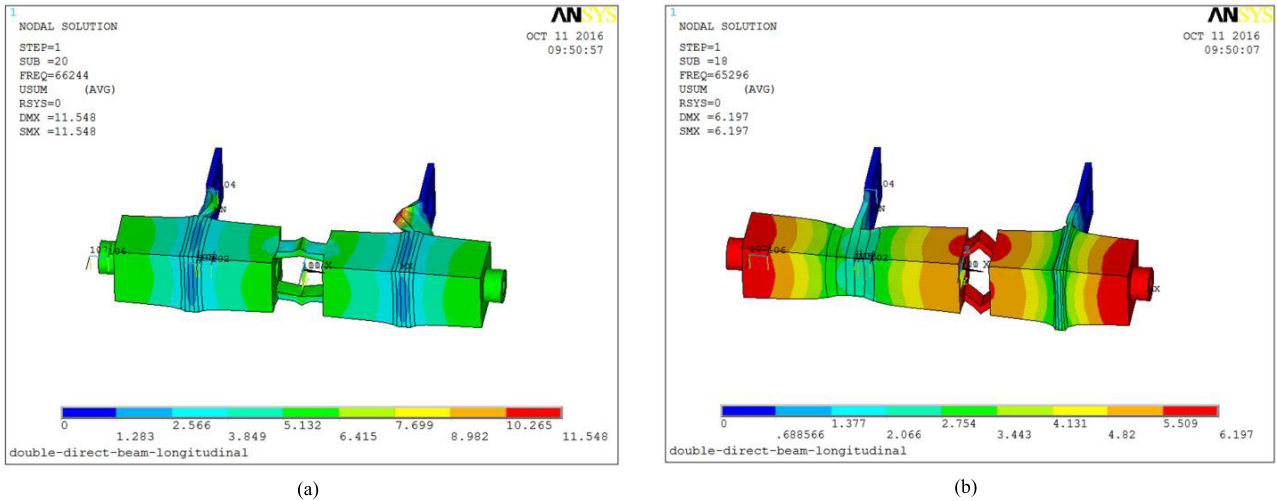
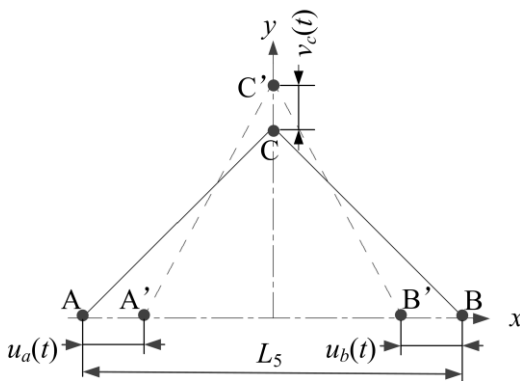FIGURE 3. Operation modes by ANSYS: (a) Symmetric mode; (b) Anti-symmetric mode.

FIGURE 4. Displacement relationships of the stator.

TABLE 1. Parameters of stator.

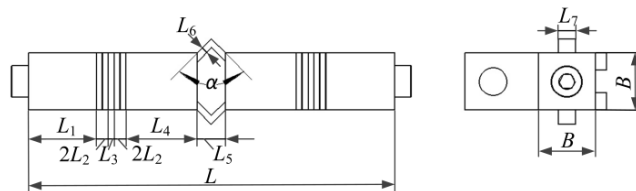|	Mass density ρ (kg/m³)	Young's modulus E (N/m²)	Poisson ratio σ
Steel	7800	2.06×10^{11}	0.3
Red copper	8900	1.08×10^{11}	0.34

FIGURE 5. Structure parameters of stator.

is illustrated. To minimize the frequency difference of the symmetric and anti-symmetric vibration modes, the vibration process of the stator was simulated by Ansys10.0®, and the influence of the triangular beam dimensions was analyzed in detail. According to the simulation results, a prototype has been fabricated, and the vibration characteristics and output performance have been investigated.

II. STRUCTURE OF THE STATOR

In order to use the vibration characteristic of mirror symmetric structure and degenerate a pair of symmetric and anti-symmetric vibration modes as an operation mode, two transducers can be set along an axis. Theoretically, the longitudinal and bending vibration modes of Langevin transducer can be utilized to construct the pair of symmetric and anti-symmetric vibration modes. To simplify the structure of the stator and the exciting method, the longitudinal vibration mode of transducer is selected as the working mode. To reduce the vibration interference of two transducers, they should be connected by low stiffness beam. A pair of thin isosceles triangular beams is selected as the connecting structure. Furthermore, they can generate the oval trajectory of the driving foot. In fact, both of the two beams can sever as two driving feet and drive two rotors or sliders.

The composite piezoelectric stator with mirror symmetric structure is shown in Fig. 1 (a). Eight rectangular piezoelectric ceramic plates polarized in the thickness direction are clamped between the beam1 and beam2 parts by bolts. Two adjacent piezoelectric ceramic plates with opposite polarization direction are set as one group and a bronze electrode plate is clamped between the two ceramic plates. The support plates are used to fix the stator. The function of two isosceles triangular connecting beams is that the displacements of two Langevin transducers in x direction (axial direction) can be transformed into the displacements in y direction (perpendicular direction), while the stator is working in longitudinal vibration mode. That is one of the merits of the triangular connecting beams. The other merit is that the stiffness of the thin triangular beams is obviously lower than the transducers, which can reduce the vibration interference of the transducers. Then by the special design, the stator with mirror symmetric structure may have a pair of symmetric and anti-symmetric vibration modes, which will be tested by FEM simulation in section IV. The oval trajectory of the driving
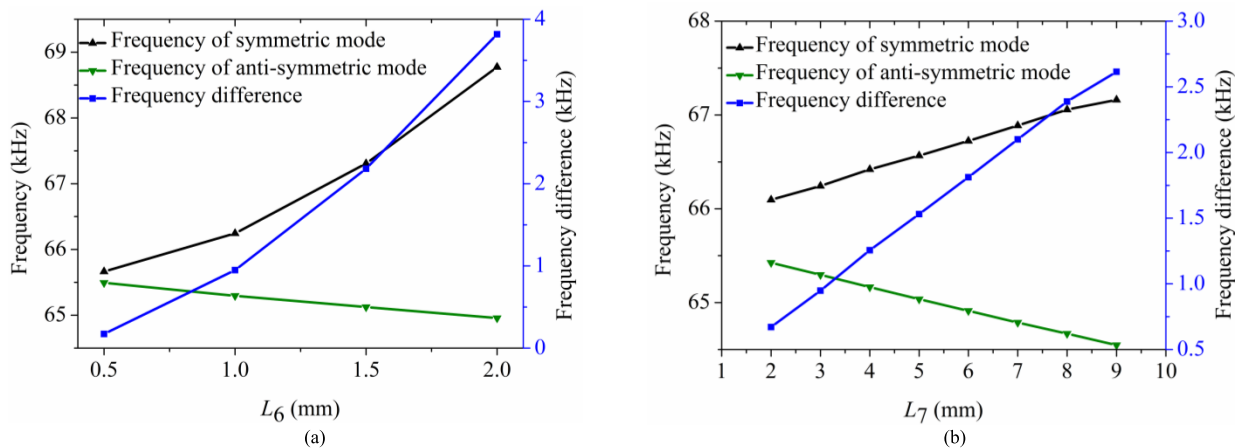
FIGURE 6. Difference of vibration frequency: (a) Frequency difference change by L_6; (b) Frequency difference change by L_7.

foot is decided by the angle α of the isosceles triangular beams, which is shown in Fig. 1 (b). The formation of trajectory will also be simulated in section IV.

The piezoelectric ceramics are polarized in the thickness direction, and the arrangement of them is shown in Fig. 2. The polarized directions are signed as "+" and "−". During the test and operation process, the support plates and the beams must be grounded for voltage input.

III. OPERATION PRINCIPLE

As the operation principle of the motor, two orthogonal vibration modes should be excited and superposed to generate an oval trajectory of the driving foot. This stator uses the hybrid mode of the symmetric 1st longitudinal and anti-symmetric 1st longitudinal vibration modes in x direction as operation mode. To verify the existence of above mentioned two modes, modal analysis was carried out. And Fig. 3 shows the simulation results of the stator. When the symmetric vibration mode as shown in Fig. 3 (a) is excited, the triangular beams transform the movements of the transducers in axial direction (x axis direction) into the movements of themselves in perpendicular direction (y axis direciton), and the vertexes of the triangular beams move upward and downward reciprocally. When the anti-symmetric vibration mode is excited, as shown in Fig. 3 (b), the vertexes of the triangular beams move in axial direction. Exciting the two operating modes simultaneously with phase difference of 90°, the oval trajectory on the vertexes of the triangular beams can be generated. To acquire maximum vibration amplitude of the stator, the piezoelectric ceramics and the support plates are set at the nodal position.

In order to explain the generation of oval trajectory of the driving foot, the triangular beam shown in Fig. 1 (b) can be simplified as Fig. 4.

While the 1st longitudinal mode of the two Langevin transducers is excited, the displacements of point A and B in axial direction can be described as:

$$\begin{cases} u_a\,(t) = \xi_a \sin \omega t \\ u_b\,(t) = \xi_b \cos \omega t \end{cases} \tag{1}$$

where ξ_a and ξ_b are the vibration amplitude of the point A and B, ω is the angular frequency of excitation. There is the relationship: $\xi = \xi_a = \xi_b$, because that the two Langevin transducers have the same structure.

According to the geometrical relationship of the triangular beam,

$$\left(\frac{L}{2}\right)^2 + \left(\frac{L}{2}\cot\frac{\alpha}{2}\right)^2 = \left(\frac{L}{2} + \frac{\Delta u}{2}\right)^2 + \left(\frac{L}{2}\cot\frac{\alpha}{2} - \Delta v\right)^2 \tag{2}$$

where $\Delta u = u_a(t) - u_b(t)$, $\Delta v = v_c(t)$.

Equation (2) can be simplified by eliminate the squares of Δu and Δv as infinitesimal of higher order. Then,

$$\frac{\Delta v}{\Delta u} = \frac{1}{2}\tan\frac{\alpha}{2} \tag{3}$$

Then, the displacement of point C can be described as:

$$\begin{cases} u_C(t) = u_A(t) + \frac{\Delta u}{2} = \frac{3u_A(t)}{2} - \frac{u_B(t)}{2} \\ \qquad \approx 5\xi\sin{(\omega t - 72.5°)} \\ v_C(t) = \Delta v = \frac{u_A(t) - u_B(t)}{2}\tan\frac{\alpha}{2} \\ \qquad = \frac{\sqrt{2}}{2}\xi\tan\frac{\alpha}{2}\sin{(\omega t - 45°)} \end{cases} \tag{4}$$

The motion trajectory of C can be given as:

$$\left(\frac{u_C}{5\xi}\right)^2 + \left(\frac{\sqrt{2}v_C}{\xi\tan\frac{\alpha}{2}}\right)^2 - \frac{2\sqrt{2}u_C v_C}{5\xi^2\tan\frac{\alpha}{2}}\cos(27.5°) = \sin^2(27.5°) \tag{5}$$

According to equation (5), the maximum displacement of point C in perpendicular direction should increase with the increase of α.

TABLE 2. Structure parameters of stator (mm).

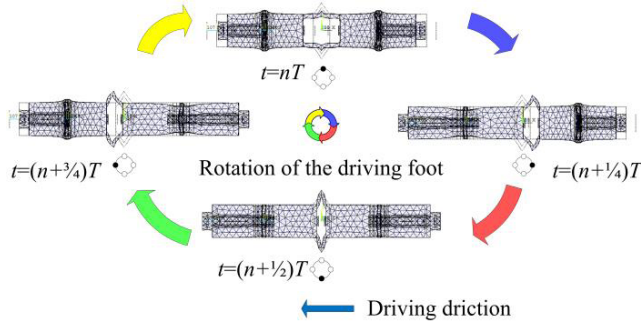| L	B	L_1	L_2	L_3	L_4	L_5	L_6	L_7	α (°)
63	10	12	1	0.5	12.5	5	1	3	90

FIGURE 7. FEM analysis of the vertex displacement of a triangular beam in one vibration cycle.
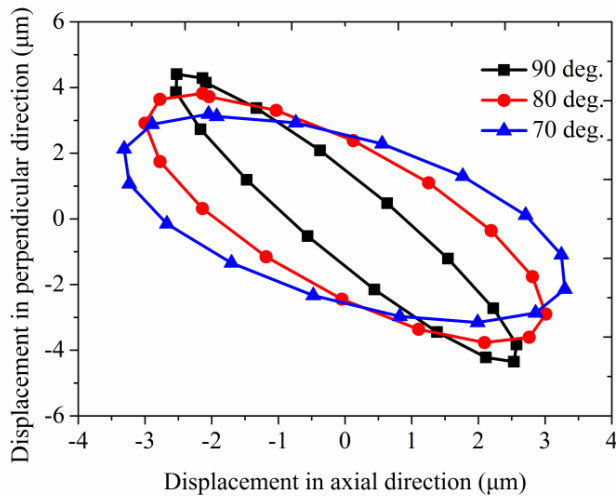
FIGURE 8. Motion trajectories of the triangular beam vertex in different angle α.

IV. FEM ANALYSIS OF THE STATOR

A finite element model was established to confirm the operation principle, adjust the frequency difference of the symmetric and the anti-symmetric first longitudinal vibration modes. In order to simplify the process of mode degeneration, the relationship between the dimensions of triangular beam and the frequency difference should be identified. So, the modal analysis of FEM was used to extract the vibration modes of stator.

Steel is chosen as the material of the beams, red copper is chosen as the material of the support plates. Table 1 lists the material parameters of the stator.

PZT-41 using the d_{33} mode is selected as the piezoelectric components. The strain matrix d, structural stiffness matrix c^E and relative permittivity coefficient ε^T of PZT ceramics
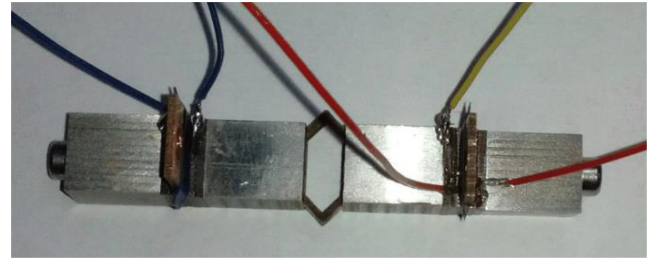
FIGURE 9. The prototype of proposed motor.

are expressed as

$$d = \begin{bmatrix} 0 & 0 & 0 & 0 & 5 & 0 \\ 0 & 0 & 0 & 5 & 0 & 0 \\ -1.6 & -1.6 & 3.3 & 0 & 0 & 0 \end{bmatrix} \times 10^{-10} \text{ C/N} \tag{6}$$

$$c^E = \begin{bmatrix} 15 & 8.4 & 6.8 & 0 & 0 & 0 \\ 8.4 & 15 & 6.8 & 0 & 0 & 0 \\ 6.8 & 6.8 & 12.9 & 0 & 0 & 0 \\ 0 & 0 & 0 & 3.3 & 0 & 0 \\ 0 & 0 & 0 & 0 & 2.8 & 0 \\ 0 & 0 & 0 & 0 & 0 & 2.8 \end{bmatrix} \times 10^{10} \text{ N/m}^2 \tag{7}$$

$$\varepsilon^T = \begin{bmatrix} 8.1 & 0 & 0 \\ 0 & 8.1 & 0 \\ 0 & 0 & 6.7 \end{bmatrix} \times 10^{-9} \text{ F/m} \tag{8}$$

The main structural parameters of stator are shown in Fig. 5.

Table 2 lists the structural parameters of the stator.

The thickness and width of the triangular beam are expressed as L_6 and L_7 in Fig. 5. As connecting beams, the stiffness of them directly affects the frequency difference of the 1st symmetric longitudinal vibration mode and the 1st anti-symmetric longitudinal vibration mode. And to minimize the frequency difference, the stiffness of the triangular beam can be reduced and the mode degeneration process can be simplified as an adjustment process of the two dimensions.

Fig. 6 (a) and Fig. 6 (b) show the curves of symmetric and anti-symmetric mode frequencies and the frequency difference with different L_6 and L_7, respectively. According to the simulation results, the frequency differences between the two modes increases with the increase of L_6 and L_7. It's because that the stiffness of the triangular beams increases with the increase of L_6 and L_7. Therefore, L_6 and L_7 should be small to reduce the frequency difference, which can provide better mode degeneration.

When all the dimensions of the stator are agree with Table 1, the resonance frequencies of the 1st symmetric and anti-symmetric longitudinal mode are 65.30 kHz and 66.24 kHz. The frequency difference of the two modes is 0.94 kHz.

The transient analysis was carried out to investigate the operation principle and test the formation of the
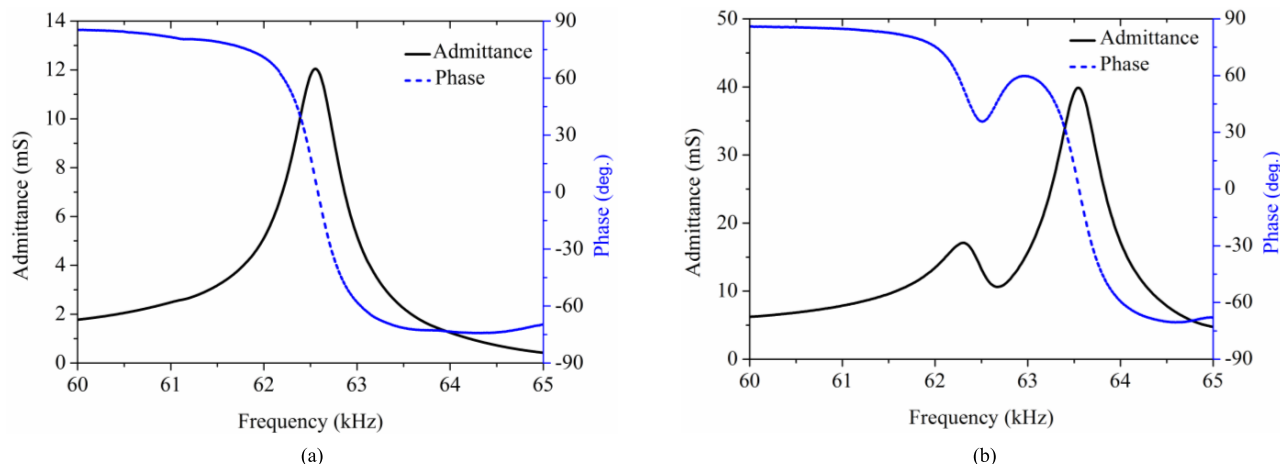
FIGURE 10. Admittance and phase characteristics of the stator with respect to the frequency: (a) Symmetric mode; (b) Anti-symmetric mode.
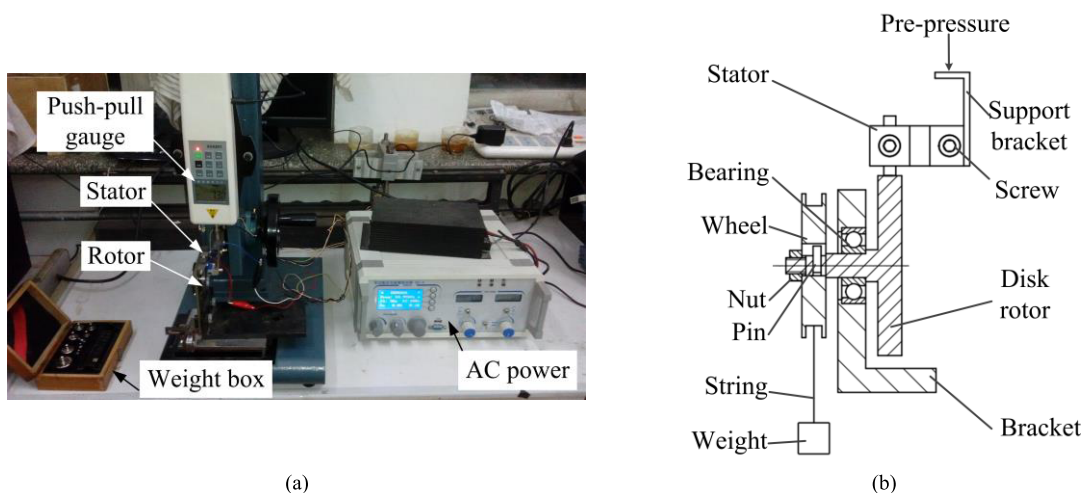

FIGURE 11. Experimental setup of the motor: (a) experiment equipment, (b) principle diagram of driving experiment.

oval trajectory. The piezoelectric ceramic plates of the two transducers were applying with two sinuous voltage signals ($V \sin\omega t$ and $V \cos\omega t$, V is the voltage amplitude, and ω is the angular frequency of voltage) having a phase difference 90°. Then, the driving foot vibrated and generated oval trajectory. Fig. 7 shows the displacement of driving foot in one vibration cycle period T ($t = nT \sim (n+1)T$, t is time).

Theoretically, the larger displacement in perpendicular direction of the vertex can generate larger output force, and the larger displacement in axial direction of the vertex can generate faster driving speed. The vibration amplitude of the vertex is also decided by the angle of the isosceles triangular beams. To identify the affection of the structure parameter angle α, the transient analysis was also performed. The oval trajectories with different angle α of the triangular beams are shown in Fig. 8. According to the simulation results, the perpendicular vibration amplitude rises up obviously with the increase of the angle α, but the axial vibration

amplitude drops down. Finally, the angle α of the prototype is set as 90°.

V. EXPERIMENTS AND DISCUSSION

According to the simulation results, an USM prototype has been fabricated, which is shown in Fig. 9. The mass of the stator is 46 g, and the whole dimension of stator is 70mm (length) × 15 mm (width) × 10 mm (thickness).

To verify the existence of the two aforementioned modes, the resonance frequency of the stator and the associated admittance of the stator were tested by an impedance analyzer (4294A, Agilent Inc., Palo Alto, CA, USA). To measure the drive admittance of the symmetric mode of the stator, all electrodes were connected to high terminal, and the metal body was connected to the low terminal of the impedance analyzer. To measure the admittance of the anti-symmetric mode, electrode A (Fig. 1 (a)), was connected to the high, and electrode B was connected to the low terminal.
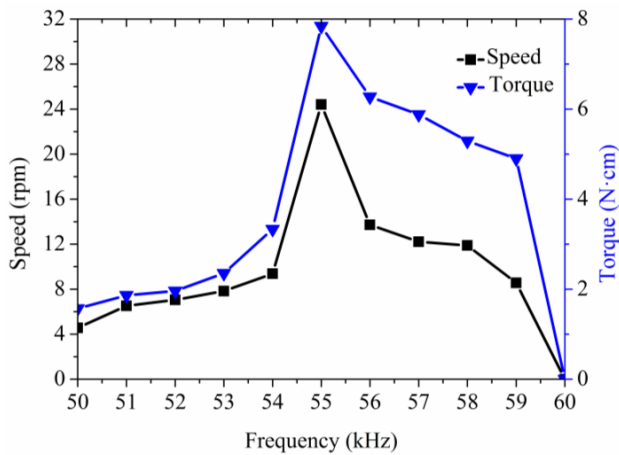
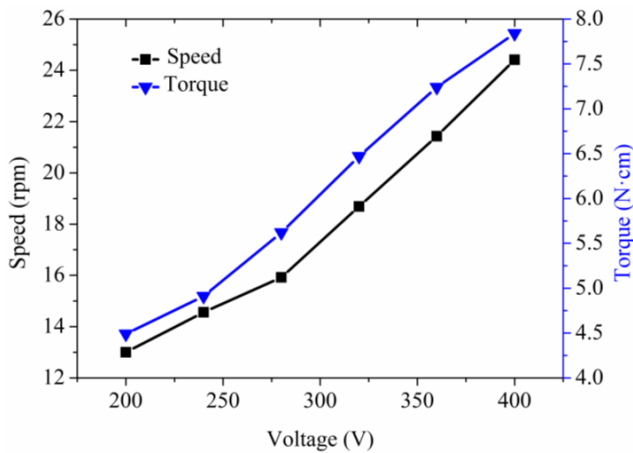**FIGURE 12.** Characteristic of speed and torque depending on the frequency.

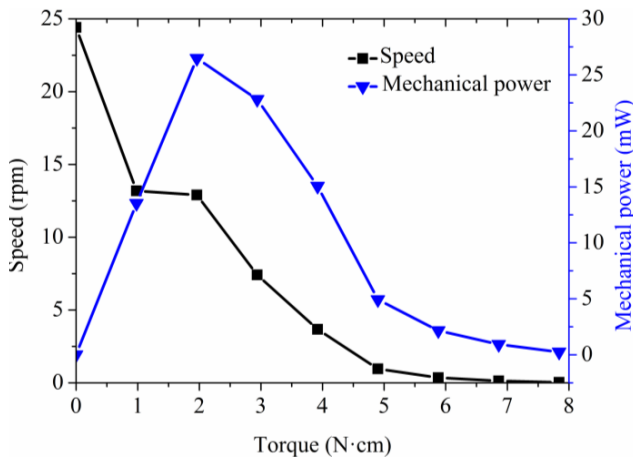**FIGURE 13.** Characteristic of speed and torque depending on the voltage.

FIGURE 14. Mechanical output characteristics.

The measured admittance and phase characteristics with respect to frequency are shown in Fig. 10. And the resonance frequencies of the stator in free condition were 62.50 kHz and 63.54 kHz, respectively. The frequency difference of two modes is 1.04 kHz and the matching result is acceptable.

To measure the speed and output torque of the USM, an experiment stage was designed and set up, which mainly includes the AC power, push-pull gauge, stator, rotor and weight. As shown in Fig. 11, the stator was connected to the push-pull gauge applying pre-pressure by moving up and down. A steel disk rotor with 50 mm diameter was fixed to facilitate contact with the stator. The weight is used to apply the torque in order to balance the one exerted by thrust force.

The driving parameters (voltage, frequency, temperature, pre-pressure, driven load, etc.) [29] directly affect the performance characteristics of USM. For most USM, the variable frequency control and the variable voltage control are two common speed control methods [30], [31]. Fig. 12. shows the characteristics of the speed and torque depending on the frequency. The pre-pressure is 8N. Under the driving voltage with the amplitude of 400 V (peak to peak), the maximum speed and torque are 24.41 rpm and 7.84 N · cm respectively, which are obtained at the resonance frequency, 55 kHz. And the effective frequency control range is 50-59 kHz.

Fig. 13 shows characteristics of the speed and torque depending on the applied voltage, with the driving frequency of 55 kHz and pre-pressure is 8N. The speed and torque increase somewhat linearly with increasing applied voltage amplitude. The fundamental cause is that the improvement of applied voltage generates larger deformation of ceramic.

Fig. 14 shows the output torque characteristics of the USM versus the speed with the exciting frequency of 55 kHz and excitation sinusoidal voltages of 400 V_{p-p}. The typical speed-torque characteristics of USM are shown, that are high speed with low torque and low speed with high torque. The mechanical power curve is concave down when the torque is lower than 5N · cm and concave up when the torque is higher than 5N · cm. The maximum mechanical power is 26.48mW at the torque of 1.96N · cm. And the no-load speed 24.41 rpm and maximum torque 7.84 N · cm can be transformed as no-load speed 63.87 mm/s and maximum thrust force 3.14 N, respectively.

VI. CONCLUSIONS

In order to minimize the dimensions of bolt-clamped type USM and acquire acceptable output performance, a new linear ultrasonic motor is proposed in this paper. Several basic and typical frequency matching methods are discussed. And as a special design, a low stiffness isosceles triangular beam structure is introduced as the connecting beam of multi transducer, which can transform the displacement in axial direction of transducers into the displacement in perpendicular direction of driving foot and reduce the vibration interference of the transducers. The numerical model of triangular beam was set up to explain the principle of displacement transformation. The operating mechanism of the stator is described. The effects of the triangular beams on the vibration frequency of the stator and the amplitude of the driving foot were analyzed and simulated by FEM analysis. According to the results of the simulation, the

triangular beam is an effective structure to generate the oval trajectory of the driving foot. And the frequency matching process of ultrasonic motor is simplified by adjusting the structure dimensions of the triangular beams. A prototype motor was fabricated and tested. The difference of first symmetric longitudinal and anti-symmetric longitudinal vibration modes is only 1.04 kHz. Driven by AC signals with the driving frequency of 55 kHz and voltage 400 V_{p-p}, the motor can provide the no-load speed 63.87 mm/s and maximum thrust force 3.14 N, respectively. Comparing with the former researched USM [26] of author, the thrust force is improved to 2.24 times, and the dimensions of the motor are reduced apparently.

Our future work focuses on expanding the driving function of the motor by variable mode excitation.

REFERENCES

[1] B. Watson, J. Friend, and L. Yeo, "Piezoelectric ultrasonic micro/milliscale actuators," *Sens. Actuators A, Phys..*, vol. 152, no. 2, pp. 219–233, Jun. 2009.

[2] K. Jong-Wook, P. Choong-Hyo, L. Jung-Hoon, J. Seong-Su, P. Jong-Kyu, and P. Tae-Gone, "Driving characteristics of octagon-type ultrasonic motor," *J. Central South Univ.*, vol. 20, pp. 71–75, Jan. 2013.

[3] Y.-L. Shi, C. Chen, and C.-S. Zhao, "Optimal design of butterfly-shaped linear ultrasonic motor using finite element method and response surface methodology," *J. Central South Univ.*, vol. 20, no. 2, pp. 393–404, Feb. 2013.

[4] S. Shao, S. Shi, W. Chen, J. Liu, and Y. Liu, "Research on a linear piezoelectric actuator using t-shape transducer to realize high mechanical output," *Appl. Sci.*, vol. 6, no. 4, p. 103, Apr. 2016.

[5] S. Dong, S. P. Lim, K. H. Lee, J. Zhang, L. C. Lim, and K. Uchino, "Piezoelectric ultrasonic micromotor with 1.5 mm diameter," *IEEE Trans. Ultrason., Ferroelect., Freq. Control*, vol. 50, no. 4, pp. 361–367, Apr. 2003.

[6] T. Mashimo, "Micro ultrasonic motor using a one cubic millimeter stator," *Sens. Actuators A, Phys..*, vol. 213, pp. 102–107, Jul. 2014.

[7] K. Takemura and T. Maeno, "Design and control of an ultrasonic motor capable of generating multi-DOF motion," *IEEE/ASME Trans. Mechatronics*, vol. 6, no. 4, pp. 499–506, Dec. 2001.

[8] C. Zhu, X. Chu, S. Yuan, Z. Zhong, Y. Zhao, and S. Gao, "Development of an ultrasonic linear motor with ultra-positioning capability and four driving feet," *Ultrasonics*, vol. 72, pp. 66–72, Dec. 2016.

[9] T. Mashimo, "Micro ultrasonic motor using a cube with a side length of 0.5 mm," *IEEE/ASME Trans. Mechatronics*, vol. 21, no. 2, pp. 1189–1192, Apr. 2016.

[10] R.-R. Geng, J. K. Mills, and Z.-Y. Yao, "Design and analysis of a novel 3-DOF spatial parallel microgripper driven by LUMs," *Robot. Comput.-Integr. Manuf.*, vol. 42, pp. 147–155, Dec. 2016.

[11] Y. Liu, W. Chen, J. Liu, and S. Shi, "Actuating mechanism and design of a cylindrical traveling wave ultrasonic motor using cantilever type composite transducer," *PLoS ONE*, vol. 5, no. 3, p. e10020, 2010.

[12] K. Asumi, R. Fukunaga, T. Fujimura, and M. K. Kurosawa, "High speed, high resolution ultrasonic linear motor using V-shape two bolt-clamped Langevin-type transducers," *Acoust. Sci. Technol.*, vol. 30, no. 3, pp. 180–186, 2009.

[13] Y. Shi *et al.*, "A new type butterfly-shaped transducer linear ultrasonic motor," *J. Intell. Mater. Syst. Struct.*, vol. 22, pp. 567–575, Apr. 2011.

[14] X. Li, Z. Yao, and R. Wu, "Modeling and analysis of stick-slip motion in a linear piezoelectric ultrasonic motor considering ultrasonic oscillation effect," *Int. J. Mech. Sci*, vol. 107, pp. 215–224, Mar. 2016.

[15] M. Guo, S. Pan, J. Hu, S. Dong, and C. Zhao, "A small linear ultrasonic motor utilizing longitudinal and bending modes of a piezoelectric tube," *IEEE Trans. Ultrason., Ferroelect., Freq. Control*, vol. 61, no. 4, pp. 705–709, Apr. 2014.

[16] X. Yang, Y. Liu, W. Chen, and J. Liu, "Miniaturization of a longitudinal–bending hybrid linear ultrasonic motor," *Ceramics Int.*, vol. 41, pp. S607–S611, Jul. 2015.

[17] L. Yang, X. Zhu, and X. Chen, "A novel type of hybrid ultrasonic motor using longitudinal and torsional vibration modes with side panels," *J. Vibroeng.*, vol. 18, no. 2, pp. 759–767, Mar. 2016.

[18] H. Al-Budairi, M. Lucas, and P. Harkness, "A design approach for longitudinal–torsional ultrasonic transducers," *Sens. Actuators A, Phys.*, vol. 198, pp. 99–106, Aug. 2013.

[19] Y. Liu, X. Yang, W. Chen, and D. Xu, "A bonded-type piezoelectric actuator using the first and second bending vibration modes," *IEEE Trans. Ind. Electron.*, vol. 63, no. 3, pp. 1676–1683, Mar. 2015.

[20] N. W. Hagood, IV, and A. J. McFarland, "Modeling of a piezoelectric rotary ultrasonic motor," *IEEE Trans. Ultrason., Ferroelect., Freq. Control*, vol. 42, no. 2, pp. 210–224, Mar. 1995.

[21] T. Peng, H. Shi, X. Liang, F. Luo, and X. Wu, "Experimental investigation on sandwich structure ring-type ultrasonic motor," *Ultrasonics*, vol. 56, pp. 303–307, Feb. 2015.

[22] J. Yan, Y. Liu, J. Liu, D. Xu, and W. Chen, "The design and experiment of a novel ultrasonic motor based on the combination of bending modes," *Ultrasonics*, vol. 71, pp. 205–210, Sep. 2016.

[23] D. Xu, Y. Liu, J. Liu, and W. Chen, "A bonded type ultrasonic motor using the bending of a crossbeam," *IEEE Access*, vol. 4, pp. 1109–1116, 2016.

[24] S. Dong *et al.*, "A small, linear, piezoelectric ultrasonic cryomotor," *Appl. Phys. Lett.*, vol. 86, p. 053501-3, Jan. 2005.

[25] Y. Shi, C. Zhao, and W. Q. Huang, "Linear ultrasonic motor with wheel-shaped stator," *Sens. Actuators A, Phys.*, vol. 161, nos. 1–2, pp. 205–209, Jun. 2010.

[26] X. Zhou, W. Chen, and J. Liu, "A novel multi-mode differential ultrasonic motor based on variable mode excitation," *Sens. Actuators A, Phys.*, vol. 230, pp. 117–125, Jul. 2015.

[27] P. Vasiljev, S. Borodinas, S.-J. Yoon, D. Mažeika, and G. Kulvietis, "The actuator for micro moving of a body in a plane," *Mater. Chem. Phys.*, vol. 91, no. 1, pp. 237–242, May 2005.

[28] X. Zhou, W. Chen, and J. Liu, "A new rotary ultrasonic motor using longitudinal vibration transducers," *Adv. Mech. Eng.*, vol. 7, no. 5, pp.1-8, May. 2015.

[29] M. Mracek and T. Hemsel, "Synergetic driving concepts for bundled miniature ultrasonic linear motors," *Ultrasonics*, vol. 44, pp. e597–e602, Dec. 2006.

[30] T. Senjyu, T. Kashiwagi, and K. Uezato, "Position control of ultrasonic motors using MRAC with dead-zone compensation," *IEEE Trans. Ind. Electron.*, vol. 48, no. 6, pp. 1278–1285, Dec. 2001.

[31] A. Ferreira and P. Minotti, "High-performance load-adaptive speed control for ultrasonic motors—II. Bidimensional analytical modelling of the stator/rotor contact," *Control Eng. Pract.*, vol. 6, no. 1, pp. 1–13, Jan. 1998.

XIANGYU ZHOU was born in Heilongjiang, China, in 1978. He received the B.S., M.S., and Ph.D. degrees from the School of Mechatronics Engineering, Harbin Institute of Technology, Harbin, China, in 2001, 2004 and 2016, respectively. From 2004 to 2010, he was an Engineer with the 21st Institute of China Electronic Science and Technology Group, Shanghai, China. Since 2016, he has been a Lecturer with the School of Advanced Manufacturing Engineering, Chongqing University of Posts and Telecommunications. His research interests include ultrasonic motor, electromagnetic motor, and bionic robot.

YI ZHANG was born in Chongqing, China, in 1966. He received the B.S. degree in precision instrument engineering from the Xi'an University of Technology in 1991, the M.S. degree from the Hefei University of Technology in 1997, and the Ph.D. degree in mechanical science and engineering from the Huazhong University of Science and Technology in 2002. Since 2006, he has been a Professor with the Chongqing University of Posts and Telecommunications. His research interests include information accessibility, multimode human-computer interaction and intelligent systems, and robotics.

● ● ●